RSC Advances

ROYAL SOCIETY OF CHEMISTRY

www.rsc.org/advances

Novel magnetic nanocomposite injectables: calcium phosphate cements impregnated with ultrafine magnetic nanoparticles for bone regeneration

Roman A. Perez[a,b], **Kapil D. Patel**[a,b], **Hae-Won Kim**[a,b,c,*]

[a]Institute of Tissue Regeneration Engineering (ITREN), Dankook University, Cheonan, 330–714, Republic of Korea

[b]Department of Nanobiomedical Science and BK21 PLUS NBM Global Research Center for Regenerative Medicine, Cheonan, 330–714, Dankook University, Republic of Korea

[c]Department of Biomaterials Science, School of Dentistry, Dankook University, Cheonan, 330–714, Republic of Korea

---

*Corresponding author: Prof. H.-W. Kim (e-mail: kimhw@dku.edu; tel: +82 41 550 3081; fax: +82 41 550 3085)

For: RSC Advances

Abstract

Self-setting calcium phosphate cements (CPCs) are some of the few injectables of bioceramic materials applicable to bone repair. Incorporation of nanoparticulates to CPCs is considered a promising process that can improve the mechanical and biological properties of CPCs. Here, we added magnetic nanoparticles (MNPs) at small contents, and examined their effects on the physico-chemical, mechanical, and in vitro biological properties of the CPC composition. The MNPs were coated with a thin silica layer and had an average size of ~80 nm. The addition of MNPs did not alter the setting reaction, but dramatically changed the crystal shape and size of the transformed hydroxyapatite, from large plate-like crystals to small needle-like crystals. Mechanical strength was significantly improved from 22 MPa to 33 MPa with the addition of only 0.1% MNPs. A striking difference in cell adhesion of rat bone marrow stromal cells was noticed by the MNPs-incorporation. The cells adhered and spread more actively to the MNP-added CPCs than to the pure CPCs with an approximately 2.5-fold and 4.5-fold increase in cell adhesion and in cell spreading area, respectively. The cell proliferative potential lasted for a longer period of up to 14 days where osteogenic differentiation, determined by alkaline phosphatase activity, was also substantially stimulated by the MNP-incorporation. The results indicate that only a small incorporation of ultrafine MNPs changed the properties of CPCs dramatically, enabling them more suitable for use in cell culture and repair of bone tissues.

Keywords: Calcium phosphate cements; nanocomposites; magnetic nanoparticles; cell adhesion; hydroxyapatite nanocrystals; bone repair

1. Introduction

Calcium phosphate cements (CPCs) are self-setting, injectable pastes that hydrolyze at body temperature into calcium deficient hydroxyapatite (HA), which has the same mineral phase as bone.[1] CPCs have been widely used for bone repair and reconstruction due to their high biocompatibility and osteoconductivity. Despite their excellent biological properties, CPCs still need improvement, particularly in their mechanical properties that match those of native bone to be applicable for load-bearing parts. Furthermore, whilst presenting excellent *in vivo* behaviors, CPCs pose a limited ability in vitro for cells to adhere to and proliferate on them. To overcome these limitations, CPCs have often been combined with additional phases, including polymers and ceramics, either in solution or in particulate form.[2]

Above all else, an interesting and promising approach is the use of nanoparticles. Nanoparticles are generally added to ceramic and polymeric matrices to produce nanocomposites aiming at improving the mechanical properties, such as increased strength and toughness.[3-6] Furthermore, nano-structured materials have been observed to stimulate cellular behaviors during initial adhesion and osteogenic differentiation.[7] While many types of nanoparticles have long been utilized as nanocomposite biomaterials for bone repair and reconstruction, very little has been investigated with respect to their application in CPCs.

To this end, we develop nanocomposite CPCs by incorporating nanoparticles. In particular, we focus on magnetic nanoparticles (MNPs) with superparamagnetic properties. In fact, MNPs have attracted much interest for a wide range of applications, such as for magnetic resonance imaging, hyperthermia treatment, and drug delivery.[8-12] Furthermore, recent studies have reported that the existence of MNPs within biomaterials had profound effects on cell proliferation and differentiation,[13-23] although the exact mechanism for the MNP-induced cellular stimulation has yet to be discovered. For instance, the MNPs incorporated to sintered bioceramic materials showed significantly enhanced cell proliferation and osteoblastic activity[18-20] When the MNPs were added to polymeric nanofibers of poly(caprolactone) (PCL), the initial cell adhesion and osteogenic differentiation were also improved.[21] A similar result in osteoblastic cell proliferation was also noticed for the poly(lactic-co-glycolic) (PLGA) porous scaffolds with incorporating MNPs.[22] The PLGA-MNP composites were also shown to increase the cell proliferation level of myoblast cells.[23]

Therefore, the addition of MNPs to the current CPC composition is considered to reap the benefits of MNPs in order to improve the properties and to extend the applications of CPCs for bone repair purposes. Here we

investigated the effects of small incorporations of MNPs on the physico-chemical and *in vitro* biological properties of CPCs.

2. Materials and Methods

2.1. Preparation of CPC powder

CPC consisted of α-TCP, which was obtained via sintering at 1400 °C and subsequent quenching of the appropriate mixture of calcium hydrogen phosphate ($CaHPO_4$, Sigma-Aldrich C7263) and calcium carbonate ($CaCO_3$, Sigma-Aldrich C4830). α-TCP was milled in a planetary mill, and 2 wt% of precipitated HA crystallites (Merck ref.1.02143) were added to seed the precipitation reaction. The α-TCP had a median particle size of 5.5 μm, as calculated via laser diffraction.

2.2. Preparation and characterization of MNPs

The synthesis of magnetic nanoparticles (MNPs) was carried out by means of a reflux method as previously described.[11,12] Briefly, 3.532 g $Fe(acac)_3$ (iron(III) acetylacetonate), 3.912 g 1,2-hexadecanediol, 10 ml of oleic acid, 10 ml of oleylamine, and 40 ml of benzyl were mixed together. The mixture was preheated to refux at 200 ^oC for 30 min while stirring, and then heated to 300 ^oC for 2 h under a nitrogen gas. The black-brown mixture was allowed to cool to room temperature and 50 ml of ethanol was added. The precipitated products were collected by centrifugation at 10,000 rpm for 5 min, washed with ethanol and dried at 50 ^oC.

The procedure of the silica-shell formation on the MNPs was also described elsewhere.[12,13] Briefly, 40.0 mg MNPs were dispersed in 2 ml of chloroform, to which 0.25 g CTAB solution in 20 ml distilled water was added and stirred at 70 ^oC for 5 h to evaporate the chloroform. A solution of 90 ml water and 3 ml ammonium hydroxide was added and then stirred at 40 ^oC. After this, a mixture of 5 ml ethyl acetate and 250 μl TEOS solution was added drop-wise, and then stirred for 5 h. The solution was decanted, and the resultant silica-coated MNPs were washed with water and ethanol and then dried overnight under vacuum.

The nanoparticle morphology was observed by transmission electron microscope (TEM; JEOL-7100). The phase and chemical bond structure of samples were examined by X-ray diffraction (XRD; Rigaku) and Fourier transform infrared spectroscopy (FTIR; Varian 640-IR), respectively.

2.3. Preparation of CPC nanocomposites

When preparing the CPC pastes, different CPC formulations were prepared by incorporating different amounts of MNPs in the liquid phase. The liquid phase was of a 2.5% Na_2HPO_4 solution. Different MNP concentrations were incorporated in the liquid phase and were sonicated until a homogenous dispersion was obtained. The amount of MNP present was calculated in terms of weight percentage with respect to the CPC powder. The MNP concentrations used were up to 5%, with pristine CPC as the control. The powder was added into the liquid phase at an L/P ratio of 0.4 ml/g. The paste that was formed was then introduced into Teflon molds (∅ = 6 mm, h = 3 mm), unless otherwise specified, and was left 7 days in water for the complete reaction into calcium deficient hydroxyapatite (CDHA).

2.4. Characterization of physico-chemical properties

The setting time of the CPC paste was measured by using the Gilmore needle method in accordance with the ASTM C266-99 standard (ASTM International C266-99, 2007). The phase composition was evaluated via XRD with Ni-filtered Cu K_α radiation. Step-scanning was performed at an integration time of 50 s with intervals of 0.017° (2θ). Peak indexing was carried out by means of JCPDS cards 29-359 for α-TCP and 9-432 for HA. Scanning electron microscopy (SEM, JEOL JSM-840) was used to investigate the microstructure of the different CPCs. The samples were sputtered with platinum prior to analysis. Infrared spectroscopy was used to determine the different bonds present in the composite. The composites were crushed to obtain a fine powder that was then mixed at a ratio of 1:100 with potassium bromide (KBr), and then analyzed with FTIR. The magnetic properties of the samples were studied using a superconducting quantum interference device (SQUID, Quantum Design MPMS-XL7) with an applied magnetic field of 620 kOe at room temperature. The magnetic properties of the particles were evaluated in terms of the saturation of the magnetization and the hysteresis loop area.

2.5. Compressive mechanical test

Cylindrical specimens (∅ = 6 mm, h = 12 mm) were prepared by introducing the pastes into Teflon molds. After a 7-day reaction in water at 37 °C, the samples were tested in a Universal Testing Machine (Instron) at a crosshead speed of 1 mm/min, and eight samples were tested for each composition.

2.6. Protein adsorption test

In order to observe the ability of the CPCs to attract proteins to the surface of the material, the disks were placed in 24-well plate and were left for 8 h in contact with 1 ml of a 500 µg/ml model protein (cytochrome c) solution. The supernatant was collected in order to measure the amount of protein that was not adsorbed into the CPC by using a UV spectrophotometer at a wavelength of 408 nm.

2.7. In vitro cell culture

Rat bone marrow stromal cells (rBMSCs) were used in the in vitro cell tests. rBMSCs were harvested from the femora and tibiae of adult rats (180–200 g) according to the guidelines approved by the Animal Ethics Committee of Dankook University. The harvested product was then centrifuged, and the supernatant was collected and suspended within a culture flask containing a normal culture medium of α-minimal essential medium (α-MEM) supplemented with 10% fetal bovine serum (FBS), 100 U/ml penicillin, 100 mg/ml streptomycin in a humidified atmosphere of 5% CO_2 with air at 37 °C. After incubation for 1 day, the medium was refreshed and cultured until the cells reached near confluence. After the subculture and after maintaining in normal culture conditions, cells from 2–3 passages were used for further tests.

Fifteen-millimeter disks were prepared for each cement group. α-TCP powder was mixed with each corresponding solution at an L/P ratio of 0.40 ml/g. The disks were left to react in water for 7 days to ensure the transformation of the α-TCP into CDHA. Tissue culture plates were used as a control, and the samples, previously sterilized by immersion for 1 h in 70% ethanol, were introduced in 24-well plates and were incubated overnight with medium.

2.8. Cell adhesion tests

In order to observe cell attachment, 2 x 10^4 cells were seeded onto each material. After 6 h, the samples were quantified by means of a CCK-8 reagent (Dojindo Molecular Technologies). CCK-8 is based on the WST-8 reaction that produces an orange formazan dye in an amount that is directly related to the number of viable cells. The medium was removed and was replaced with 200 µl of serum-free medium followed by an addition of 20 µl of CCK-8 solution. The reagent was left to react for 2 h, and then the reactant was read at an absorbance of 450 nm.

The cell morphology during initial attachment was observed via confocal laser scanning microscopy using an LSM 510 apparatus (Zeiss Goettingen). At each culture period, the cells were fixed with 4% paraformaldehyde solution and stained with Alexa Fluor 546 conjugated Phalloidin (Molecular Probes) and Prolong Gold antifade reagent with 4',6-diamidino-2-phenylindole (DAPI; Molecular Probes). Based on the fluorescent images, the cell spreading area was quantified using ImageJ Software (NIH, Bethesda, MD), and the average value (area per cell) was considered.

2.9. Cell proliferation

Relative cell numbers were evaluated at 1, 7, and 14 days using the CCK-8 assay. After 7 and 14 days, SEM images were taken in order to characterize the cell morphology. Samples prepared for the SEM were initially washed in phosphate buffer of 0.1 M, pH 7.4, fixed with 2.5% Glutaraldehyde (GA, Sigma-Aldrich G400-4) solution in PBS, and then washed and maintained in 0.1M phosphate buffer. Different ethanol solutions were used to dehydrate the samples (50, 70, 90, 96, and 100% ethanol). Finally, hexamethyldisilazane (HDMS, Fluka 52620) was used for complete dehydratation, and the samples were air-dried afterwards.

2.10. Alkaline phosphatase determination

The retention of the osteoblastic phenotype was evaluated by measuring alkaline phosphatase (ALP) activity. A colorimetric method was used that is based on the conversion of p-nitrophenyl phosphate into p-nitrophenol in the presence of alkaline phosphatase. The lysates obtained in the previous section were mixed with 2-Amino-2-methyl-1-propanol buffer (Sigma Diagnostics Inc., A9226) and phosphatase substrate solution (Sigma, 4 mg/ml P5994) and were incubated for 30 minutes at 37 °C. The reaction was stopped with 0.05 M NaOH and the production of p-nitrophenol was determined by measuring absorbance at 405 nm. The values were calibrated to a standard curve prepared from known concentrations of *p*-nitrophenol (Sigma, N7660) and the results for alkaline phosphatase activity were normalized to the number of cells on each sample.

2.11. Statistical analysis

The cell experiments were performed twice using three replicates for each condition. Statistical analysis was carried out with a significance level of 5%. One way analysis of variance (ANOVA) with a Fisher post-hoc test was conducted. The data are expressed as mean ± standard deviation.

3. Results

3.1. Physico-chemical properties

First, the silica-coated MNPs used for the cement preparation were characterized. The morphology of the nanoparticles was examined by TEM. The native form of MNPs without silica coating was spherical with uniform size of ~10 nm. After the silica coating, the nanoparticles showed a size of approximately 80 nm, where a core Fe_3O_4 magnetite (arrowed) was covered with a silica layer (Fig. 1b). The XRD patterns of the nanoparticles showed characteristic peaks of Fe_3O_4 magnetite as well as a broad silicate amorphous peak ($2\theta \sim 20^o$) (Fig. 1c). Furthermore, the FTIR spectra of the nanoparticles revealed the existence of bands related with silica (1080, 800, and 450 cm^{-1}) along with Fe-O band (600-560 cm^{-1}) (Fig. 1d).

Next, the setting time for the cements containing different MNP contents was measured. The setting time was observed to be around 13 min regardless of the specific composition (Fig. 2a). After immersion in water for 7 days, the phase change of the cements was examined via XRD (Fig. 2b). The results indicate that there is a substantial conversion of the α-TCP (initial phase) into hydroxyapatite (HA), with only small remnants of α-TCP. The HA peaks appeared broaden as the amount of MNPs increased. The FTIR spectra of the water-immersed cements (Fig 2c) showed typical bands for calcium-deficient HA, including bands related with phosphate at 844, 1006, 1026, 1085, 1130 cm^{-1}, and those associated with the hydroxyl group at 1210 and 3500 cm^{-1}. There were no characteristic peaks related to the MNPs, presumably due to the low MNP content below the detection limit.

The SEM morphology of the cements was examined after soaking in water for 7 days (Fig. 3). Pure CPC showed platelet-like large crystallites, which is typical for calcium deficient HA derived from conventional CPCs. The addition of MNPs showed a considerable effect on the crystal size of the HA. With 0.1% MNPs, some needle-like small crystals were also observed together with larger crystals. With 1% MNP, the needle-like crystal pattern was dominant. The existence of MNPs was not readily detectable in the SEM micrographs, possibly due to the nature of tiny MNPs' size (~20 nm) and the pronounced development of HA nanocrystallite precipitation.

The compressive mechanical strength for CPCs containing different MNP contents is shown in Fig. 4. The strength of the CPCs was improved significantly when the MNPs were added at small quantities, reaching a peak at 0.1%. However, with further additions, the strength was shown to decrease gradually.

The magnetic properties of the CPCs were investigated by observing the magnetization curve of samples according to variations in the magnetic field (Fig. 5). While pure CPC did not show any magnetization behavior, the MNP-incorporated CPCs exhibited typical magnetization behaviors with respect to the magnetic field. The saturation magnetization was of 0.05 emu/g and 0.35 emu/g for the 0.1% MNP and 1% MNP, respectively.

The protein adsorption behavior onto the cement samples was examined after soaking the cement samples in a protein medium for 8 h, as shown in Fig. 6. The protein adsorption increased as the incorporated MNP content increased with 85 μg for 0% MNP, 110 μg for 0.1% MNP, and 130 μg for 1% MNP.

3.2. Responses of rBMSCs to cements

The *in vitro* cellular responses to the different CPCs were assessed by using rBMSCs. Fig. 6 shows the initial cell adhesion level onto CPCs with different MNP contents. The number of adhered cells, counted with a hemocytometer during culture for 6 h, was significantly higher as the MNP content increased up to 1%, which however, was reduced again with further additions of MNPs. Even so, the cements containing higher contents of MNPs had significantly higher cell adhesion level than the pure CPC. The increase with 0.1% and 1% MNP addition was of ~1.5-fold and 3-fold, respectively, when compared to the pure CPC.

The cell adhesion and spreading morphology was examined via fluorescence microscopy during culture for 6 h, as presented in Fig. 8. While cells on pure CPC showed somewhat limited spreading morphology, those on CPCs with 0.1% MNP had highly extended cytoskeletal processes, and such cell behaviors were more pronounced with 1% MNP addition. The cell spreading area, quantified based on the fluorescence images, showed significant improvement with MNP addition: ~2.5-fold and 4.5-fold improvements with the addition of 0.1% and 1% MNP, respectively.

The proliferation of cells on the different CPCs was examined during culture for up to 14 days (Fig. 9a). Up to 7 days, no significant differences were apparent in the cell numbers between the cement groups. However, at day 14, the cell number was significantly higher in the cements containing MNPs, suggesting that the cells had proliferated better during 7 to 14 days on the MNP-incorporated CPC samples. The cell morphology was also

monitored via SEM (Fig. 9b). While cells showed limited cell-to-cell contacts at day 7, those at day 14 exhibited substantial cellular bridges with elongated cytoskeletal processes. The cells on MNP-incorporated CPCs appeared to have more elongated and fibrous-structured cellular processes.

ALP activity was determined as an index of the osteogenesis of rBMSCs during culture for up to 14 days. In pure CPC, the total ALP levels increased from 3 to 7 days and then stabilized at 14 days. On the other hand, in the MNP-added CPCs, the total ALP level did not increase from 3 to 7 days, and then was observed to significantly increase on day 14 (Fig. 10a). This trend was more noticeable with the addition of higher MNP content. The ALP level was then normalized with respect to the cell number at each culture period (Fig. 10b). Whilst the ALP level was relatively high in the early culture periods of pure CPCs (3 and 7 days), with a subsequent decrease at 14 days, the low ALP levels in the MNP-incorporated CPCs substantially increased at day 14. As a result, the MNP-added CPCs had higher cell proliferation and ALP activity, particularly at 14 days.

4. Discussion

The present study first examined the effects on the physico-chemical properties of CPCs with only small incorporations of MNPs. One previous study has touched on the theme of MNP/CPC composites.[17] In the study, the MNPs were in native form without the coverage of silica layer, which however, was implemented to improve the dispersibility and biocompatibility.[7,18] We added MNPs in very small quantities of only up to a few %, which was also quite different from the previous study where the additions of MNPs were as high as 10-20%. It was thought that the surface-related properties of the tailored nanoparticles might be substantially altered, and this could be reasoned to the use of different nanoparticle additions and the consequent effects on the properties of cements.

First, the initial setting reaction of the CPCs was not much altered due to the addition of tailored MNPs. The small fraction of MNPs is considered not to alter the flow properties the CPC paste since most MNPs will be present in the liquid phase between the α-TCP particles during the setting process, which is not likely to hamper the dissolution and precipitation reactions.[17] Furthermore, the MNPs used in this work were tailored to have a thin silica coating layer that prevents the agglomeration of the MNPs.[7] The homogeneous dispersion of nanocomponents within the host matrix is of special importance to obtain satisfactory properties that are the goal of using a nanocomposite approach.

A striking difference in the HA crystal morphology was noticed to result from the incorporation of MNPs. The platelet (~500–600 nm x 500–600 nm) crystalline morphology, generally noticed in conventional CPCs, changed to needle-like morphology (~500–600 nm length x tens of nm in diameter) with an increase of the MNP content. In fact, the MNPs could not be discernible from the SEM images primarily due to that the CDHA might have precipitated from the MNPs, shielding the nanoparticulate structure. Therefore, the MNPs are thought to act as a nucleation site of CDHA crystallization. The increase in MNP content could thus increase the nucleation rate, consequently reducing the crystal size of CDHA. Along with the altered crystal shape, the size of crystals thus also changed. While XRD and FT-IR patterns could not do feature such dramatically-changed crystal morphology, the XRD peak intensities of the calcium-deficient HA appeared to be smaller in the MNP-added CPCs, indicating smaller crystals domains. Previous results also showed broader HA peaks in the presence of collagen that was correlated with a smaller crystal domain in collagen-CPCs.[25]

Along with the change in the crystal morphology, there was also a noteworthy change in the mechanical strength of the CPCs. The addition of only 0.1% MNPs showed significant improvements from 22 MPa to 33 MPa in mechanical strength. This increase, however, was not observed with higher additions (more than 0.2%) of MNPs. It is thus considered that the 0.1% of MNPs was only effective in strengthening the CPC composition after setting. The exceptionally small quantity of CPCs had a significant effect on the mechanical strength, which is quite notable. The major reason for this mechanical strengthening phenomenon related with small quantity of MNPs is deemed to be the homogenous distribution of the MNPs. At higher MNP contents (more than 0.2%) the dispersibility could be reduced, rather the nanoparticles would be agglomerated, which consequently resulted in negating the reinforcing role of the nanoparticles dispersed in CPC matrix.[26] Since MNPs added to CPCs were not observed to be directly involved in the setting reaction, any effective chemical bonds that provide additional strength are not expected, limiting the threshold of the MNPs to very small quantities. Therefore, further study might be of value to engineer the MNP surface properly to enable effective chemical interactions with the CPC crystals during the setting reactions.

The addition of MNPs to CPCs had the most notable effects in the initial cell adhesion behaviors, including cell adhesion and spreading process. As was observed, the initial cell adhesion was very poor (~20% of culture dish control) on pure CPCs as was usual, but was substantially improved on the MNP-incorporated CPCs with a 1.5 and 2.5-fold increase with 0.1 and 1% MNP, respectively. Cell spreading morphology and cytoskeletal extensions were

also substantially improved with the addition of the MNPs, overcoming the poor cell adhesion and spreading nature of CPCs to a great extent. These significant improvements in the initial cell adhesion event are considered to be primarily due to the altered surface morphology, i.e., the change in surface crystal shape from platelet to needle-like structures as well as the decrease in the crystal size. The decreased crystal size will increase the surface area where protein molecules involved in the cellular adhesion can adhere more, possibly increasing the cellular recognition sites and the adhesion processes. The protein study performed using cytochrome C suggests that the MNP-incorporated CPCs might have an increased surface area when compared to pure CPCs. Although we cannot extrapolate these observations to assume there is a similarity to adhesive proteins like fibronectin, the results do imply the possible differences in adhesive protein adsorptions and the resultant initial cellular events.

While the MNP-incorporated CPCs significantly stimulated cell adhesion, the subsequent proliferative capacity was not substantially altered, particularly during the initial culture periods (up to 7 days). Rather, the cells on the MNP-incorporated CPCs exhibited great potential for proliferation during days 7 to 14, leading to a significant difference at this time. It is interesting to compare these results with those from other reports on MNP-incorporated biomaterials, such as hydroxyapatite dense ceramics and polycaprolactone porous scaffolds, where the major effects of the MNPs were noticed during the cell proliferative stage.[6,19,21] The MNP contents used in this study were much smaller (at most a few %) than those from previous reports (up to 20%). Therefore, the samples used in the previous studies should have excellent magnetic properties, possibly leading to magnetism-related alterations of cell behaviors, which however, might be less influential in the present materials. The significant improvement in cell adhesion with little impact on cell proliferation that was observed in this study is in part considered to be a result of the small quantity of MNPs incorporated, which changed the surface nanotopology more than the alteration in the magnetism-induced environments, demonstrating the discrepancy of our results with those from other studies on magnetic biomaterials. However, although the cell proliferation could be improved with higher additions, the possible compensation in mechanical properties needs also to be considered in choosing optimal contents of MNPs.

The osteogenic differentiation of rBMSCs on the MNP-incorporated CPCs, as confirmed by the ALP activity, was very limited during the initial culture periods (up to 7 days). However, osteogenesis significantly increased at day 14, demonstrating that the cells underwent substantial differentiation during culture for 7 to 14 days. On the other hand, the cells on pure CPCs exhibited relatively higher ALP activity in the early stage up to 7 days, but had little increase further up to 14 days. It initially appeared that pure CPCs induced rBMSCs to engage in

earlier osteogenesis than MNP-incorporated CPCs. However, the cell proliferation results indicated that cells in all CPC groups were predominantly in the proliferative stage even up to day 14, and thus the expression of ALP should not be high enough to indicate a subsequent slow-down since ALP production is known to decrease when the cells are predominantly engaged in the maturation stage of osteogenesis.[27,28] As demonstrated, the MNPs added to the CPCs significantly improved the cellular responses. Regarding this improvement, two possibilities are reasoned. One is the magnetic properties of MNPs; the magnetic induced cell stimulations have also previously been resported in other scaffolding systems, including MNP-added polymers and hydroxyapatite ceramics, although the exact mechanism on this is yet to be elucidated.[6,19,21] The other possibility is the morphological change in the nano-microstructure of the cements. The MNP-added nanocomposite form of CPCs enabled the formation of much finer nano-microstructure, which might enhance the binding sites for adhesive proteins and the subsequent cellular processes.

In fact, CPCs are considered to be generally poor at harboring cells on their surface and at providing ideal conditions for cellular proliferation and rapid confluence, which have thus been considered to be limitations for the *in vitro* culture of sufficient tissue cells to provide adequate cellular populations for tissue engineering. Therefore, the MNP-incorporated CPCs are believed to be at least a more effective substrate that can induce faster cell anchorage, spreading, and proliferation during certain time periods, after which cellular differentiation can be potentially meaningful. Future in-depth studies on osteogenic differentiation are considered to be warranted.

5. Conclusions

The effects of magnetic nanoparticles (MNPs) added to CPC composition were investigated. There was a significant improvement in the mechanical strength with only a small addition of MNPs (0.1%). While MNPs have little effects on the setting reaction, they changed the HA crystal shape and size dramatically from large platelets to small needle-like structures. The most significant change was noticed in the cellular adhesion processes. The MSCs adhered and spread much better on the MNP-incorporated CPCs, and the cell proliferative potential lasted a longer period of time. While further in-depth biological assessments are required, the current study suggests the MNPs-incorporated CPCs have some potential to be a new class of nanocomposite injectable system for bone repair and regeneration.

Acknowledgment: This study was supported by grants from the Priority Research Centers Program (2009-0093829), National Research Foundation, South Korea.

Figure captions

Figure 1. Characteristics of MNPs used for the preparation of cements. (a) TEM image of native form of MNPs without silica coating. (b) TEM image after silica coating showing magnetite core (arrowed) shelled with silica layer. (c) XRD patterns and (d) FTIR spectra of the prepared nanoparticles.

Figure 2. Physico-chemical characteristics of the CPCs containing different MNP contents in the composition. a) Initial setting time measured with a Gilmore needle, b) X-ray diffraction of the CPCs after 7 days of reaction in water with the initial reagent α-TCP, c) FT-IR of the transformed CPCs.

Figure 3. SEM micrographs of the fractured cement samples containing different MNP contents after 7 days of reaction in water. The crystal size reduction with an increase in the MNP content was notable.

Figure 4. Mechanical strengths of the CPCs containing different MNP contents. Statistical significant difference was noted as different alphabet character.

Figure 5. Magnetization curves of the CPCs containing different MNP contents.

Figure 6. Protein (cytochrome C) adsorption to the CPC samples containing different MNP contents, as assayed during 8 h bath in protein medium. Statistical significance difference was noted ($*p < 0.05$).

Figure 7. Initial cell adhesion level quantified by measuring the number of adhered cells during culture for 6 h. Data were represented after normalized to culture dish control. Statistical significant difference was noted as different alphabet character.

Figure 8. Cell adherence and spreading morphology at 6 h shown by fluorescence microscopy with the cell spreading area quantified. (Scale bar in the fluorescence images = 100 μm). Statistical significance difference was noted ($*p < 0.05$).

Figure 9. (a) Cell proliferation on the cement samples during culture for 3, 7, and 14 days, as measured by counting the cell number, and (b) cell growth morphology examined by SEM (scale bar = 50 μm). Statistical significance difference was noted ($*p < 0.05$).

Figure 10. ALP activity of the cells; (a) total ALP and (b) normalized to cell number. Statistical significance difference was noted ($*p < 0.05$).

References

1. M. P. Ginebra, M. Espanol, E. B. Montufar, R. A. Perez and G. Mestres, *Acta Biomater*., 2010, 6, 2863–2873.

2. R. A. Perez, H. W. Kim and M. P. Ginebra, *J. Tissue Eng.*, 2012, 3, 2041731412439555.

3. A. A. R. De Oliveira, S. M. de Carvalho, M. de F. Leite, R. L. Oréfice and M. de M. Pereira, *J. Biomed. Mater. Res. B Appl. Biomater*., 2012, 100, 1387–1396.

4. R. A. Perez, A. El-Fiqi, J. H. Park, T. H. Kim, J. H. Kim, H. W. Kim, Acta Biomater., 2014, 10, 520–530.

5. S. I. Roohani-Esfahani, S. Nouri-Khorasani, Z. F. Lu, R. C. Appleyard and H. Zreiqat, *Acta Biomater.*, 2011, 7, 1307–1318.

6. A. Gloria, T. Russo, U. D'Amora, S. Zeppetelli, T. D'Alessandro, M. Sandri, M. Bañobre-López, Y. Piñeiro-Redondo, M. Uhlarz, A. Tampieri, J. Rivas, T. Herrmannsdörfer, V. A. Dediu, L. Ambrosio and R. De Santis, *J. R. Soc. Interface*, 2013, 10, 20120833.

7. R. K. Singh, T. H. Kim, K. D. Patel, J. C. Knowles and H. W. Kim, *J. Biomed. Mater. Res. A*, 2012, 100, 1734–1742.

8. J. Kim, H. S. Kim, N. Lee, T. Kim, H. Kim, T. Yu, I. C. Song, W. K. Moon, T. Hyeon, *Angew. Chem. Int. Ed.* 2008, 47, 8438 –8441.

9. R. A. Pérez, J. E. Won, J. C. Knowles and H. W. Kim, *Adv. Drug. Deliv. Rev.*, 2013, 65, 471–496.

10. S. F. Medeiros, A. M. Santos, H. Fessi and A. Elaissari, *Int. J. Pharm*., 2011, 403, 139–161.

11. S. Sun, H. Zeng, D. B. Robinson, S. Raoux, P. M. Rice, S. X. Wang and G. Li, *J. Am. Chem. Soc*., 2004, 126, 273–279.

12. J. J. Kim, R. K. Singh, S. J. Seo, T. H. Kim, J. H. Kim, E. J. Lee, H. W. Kim, *RSC Adv*., 2014, 4, 17325-17336.

13. Y. Yamamoto, Y. Ohsaki, T. Goto, A. Nakasima and T. Iijim, *J. Dent. Res.*, 2003, 82, 962–966.

14. Q. C. Yan, N. Tomita and Y. Ikada, *Med. Eng. Phys*., 1998, 20, 397–402.

15. B. Chalidis, N. Sachinis, A. Assiotis and G. Maccauro, *Int. J. Immunopathol Pharmacol*, 2011, 24, 17–20.

16. T. Takano-Yamamoto, M. Kawakami and M. Sakuda, *J. Dent. Res*., 1992, 71, 1920–1925.

17. M. D. Vlad, L. J. del Valle, M. Barracó, R. Torres, J. López and E. Fernández, *Spine*, 2008, 33, 2290–2298.

18. Y. Wu, W. Jiang, X. Wen, B. He, X. Zeng, G. Wang and Z. Gu, *Biomed Mater,* 2010, 5, 15001.

19. S. Panseri, C. Cunha, T. D'Alessandro, M. Sandri, A. Russo, G. Giavaresi, M. Marcacci, C. T. Hung and A. Tampieri, *PLoS One*, 2012, 7, e38710.

20. N. Bock, A. Riminucci, C. Dionigi, A. Russo, A. Tampieri, E. Landi, V.A. Goranov, M. Marcacci and V. Dediu, *Acta Biomater,* 2010, 6, 786-796.

21. R. K. Singh, K. D. Patel, J. H. Lee, E. J. Lee, J. H. Kim, T. H. Kim, H. W. Kim, *PLoS One*, 2014, 9, e91584.

22. K. Lai, W. Jiang, J.Z. Tang, Y. Wu, B. He, G. Wang and Z. Gu, *RSC Advances,* 2012, 2, 13007-13017.

23. B. Chen, Y. Liang, W. Wu, J. Cheng, G. Xia, F. Gao, J. Ding, C. Gao, Z. Shao, G. Li, W. Chen, W. Xu, X. Sun, L. Liu, X. Li and X. Wang, Int J Nanomedicine, 2009, 4, 251-259.

24. S. Kwon, R. K. Singh, R. A. Perez, E. A. Abou Neel, H. W. Kim and W. Chrzanowski, *J. Tissue Eng*., 2013, 4, 2041731413503357.

25. R. A. Perez, G. Altankov, E. Jorge-Herrero and M. P. Ginebra, *J. Tissue Eng. Regen. Med*., 2013, 7, 353-361.

26. R. A. Perez and M. P. Ginebra, *J. Mater. Sci. Mater. Med.,* 2013, 24, 381-393.

27. R. K. Jaiswal, *J. Biol. Chem*., 2000, 275, 9645–9652.

28. P. Müller, U. Bulnheim, A. Diener, F. Lüthen, M. Teller, E. D. Klinkenberg, H. G. Neumann, B. Nebe, A. Liebold, G. Steinhoff and J. Rychly, *J. Cell Mol. Med*., 2008, 12, 281–291.

Figures

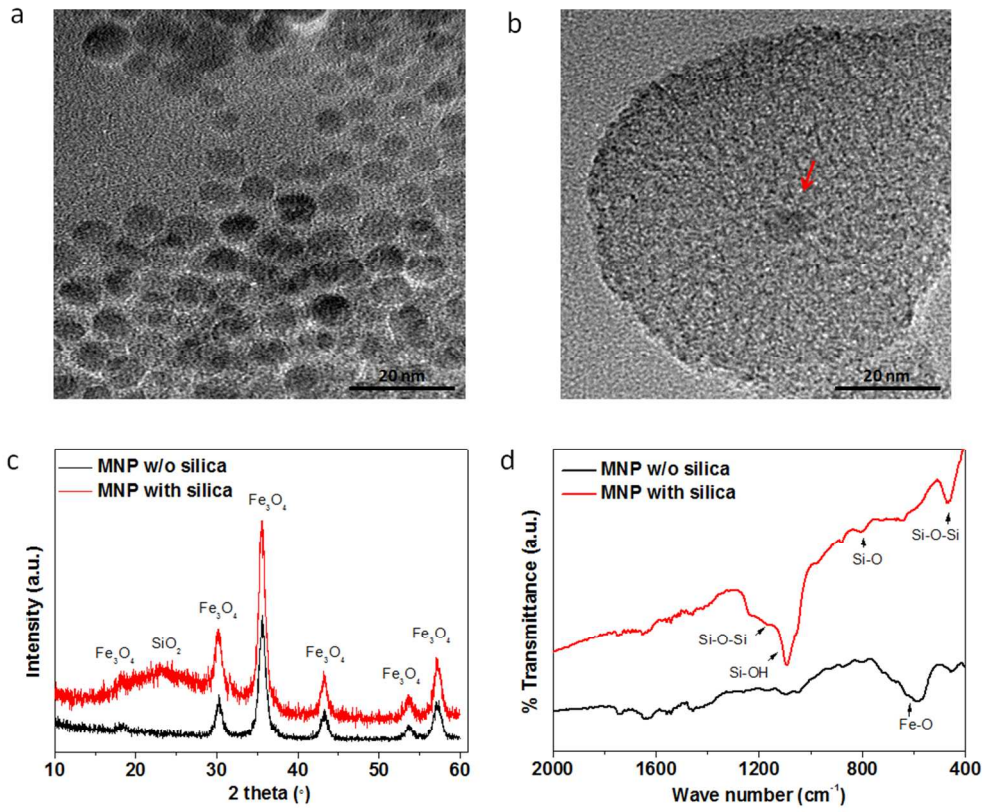

Figure 1. Characteristics of MNPs used for the preparation of cements. (a) TEM image of native form of MNPs without silica coating. (b) TEM image after silica coating showing magnetite core (arrowed) shelled with silica layer. (c) XRD patterns and (d) FTIR spectra of the prepared nanoparticles.

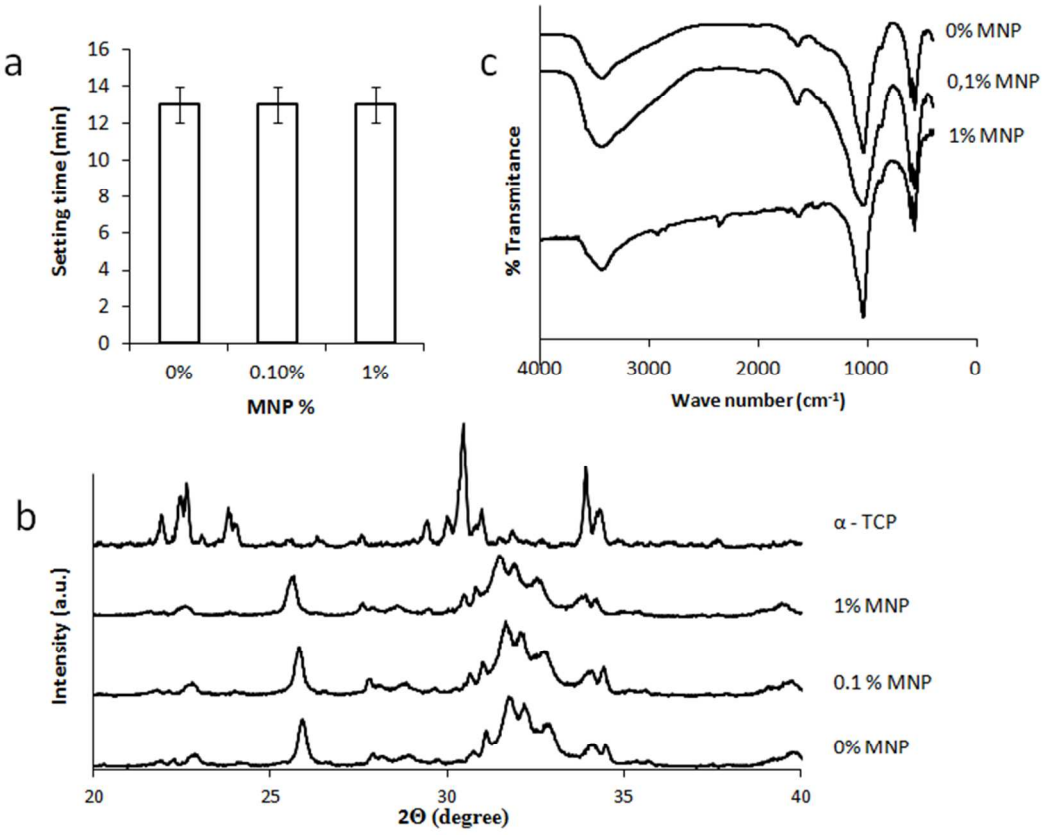

Figure 2. Physico-chemical characteristics of the CPCs containing different MNP contents in the composition. (a) Initial setting time measured with a Gilmore needle, (b) X-ray diffraction of the CPCs after 7 days of reaction in water with the initial reagent α-TCP, and (c) FT-IR of the transformed CPCs.

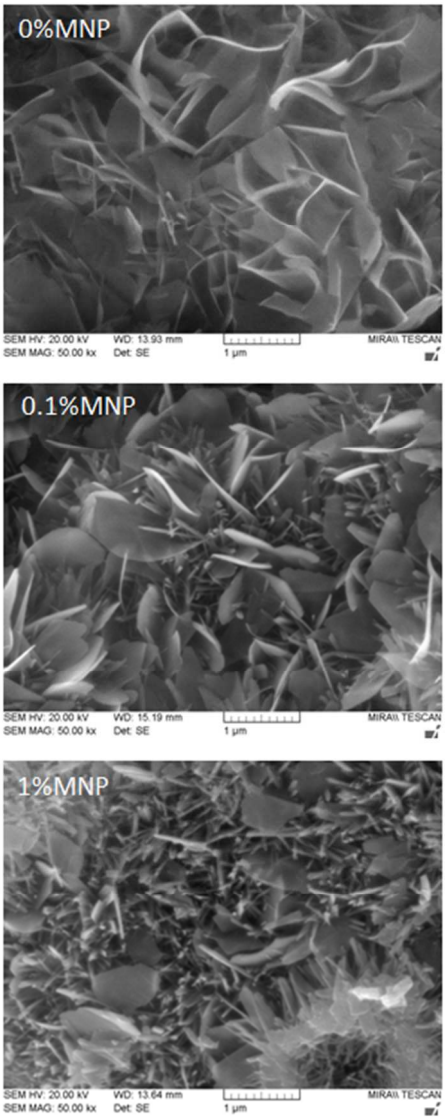

Figure 3. SEM micrographs of the fractured cement samples containing different MNP contents after 7 days of reaction in water. The crystal size reduction with an increase in the MNP content was notable.

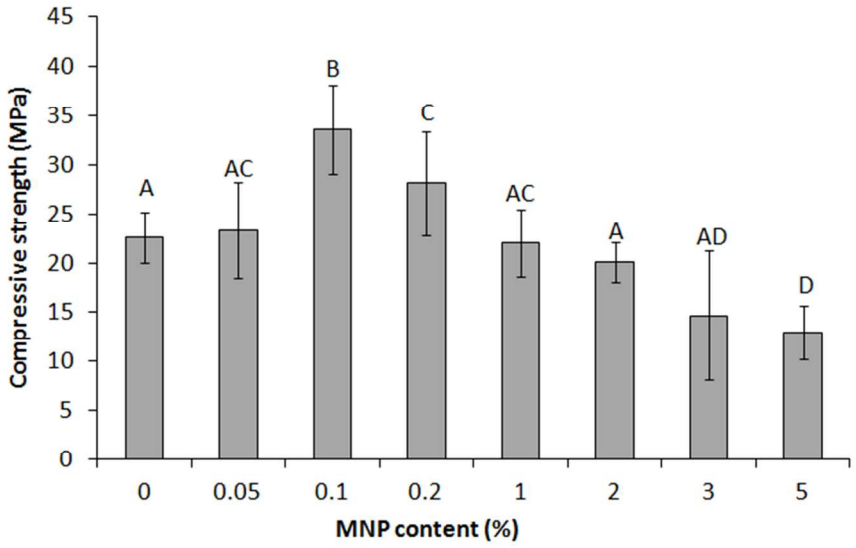

Figure 4. Mechanical strengths of the CPCs containing different MNP contents. Statistical significant difference was noted as different alphabet character.

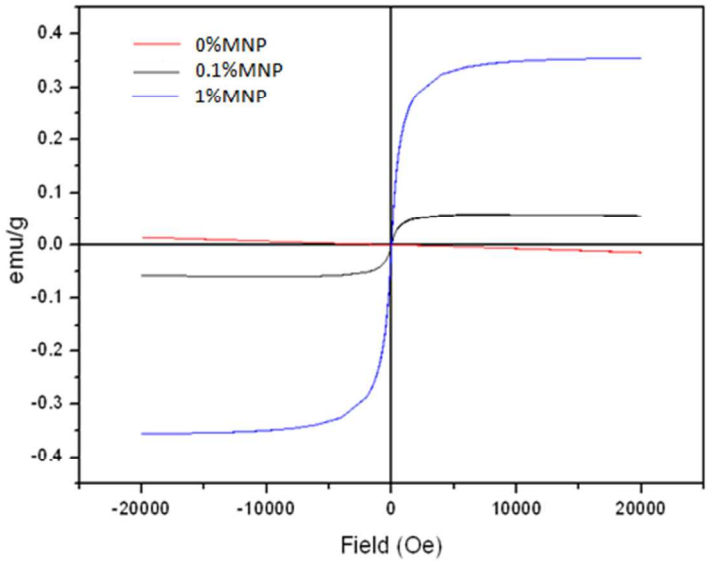

Figure 5. Magnetization curves of the CPCs containing different MNP contents.

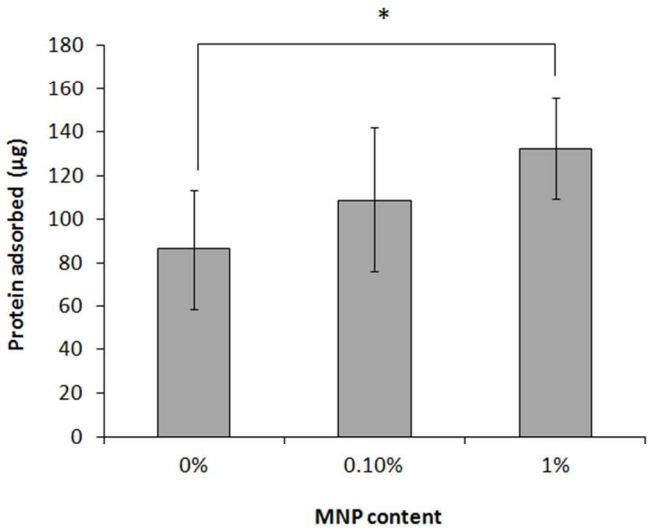

Figure 6. Protein (cytochrome C) adsorption to the CPC samples containing different MNP contents, as assayed during 8 h bath in protein medium. Statistical significance difference was noted (*$p < 0.05$).

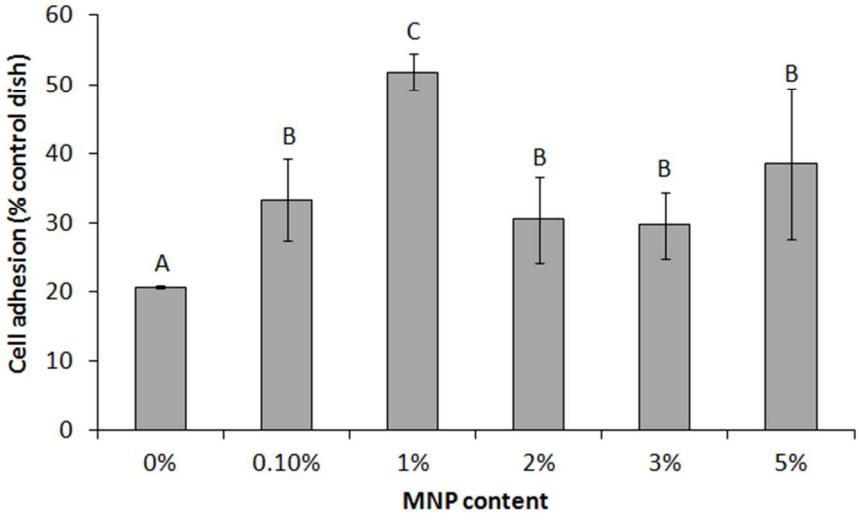

Figure 7. Initial cell adhesion level quantified by measuring the number of adhered cells during culture for 6 h. Data were represented after normalized to culture dish control. Statistical significant difference was noted as different alphabet character.

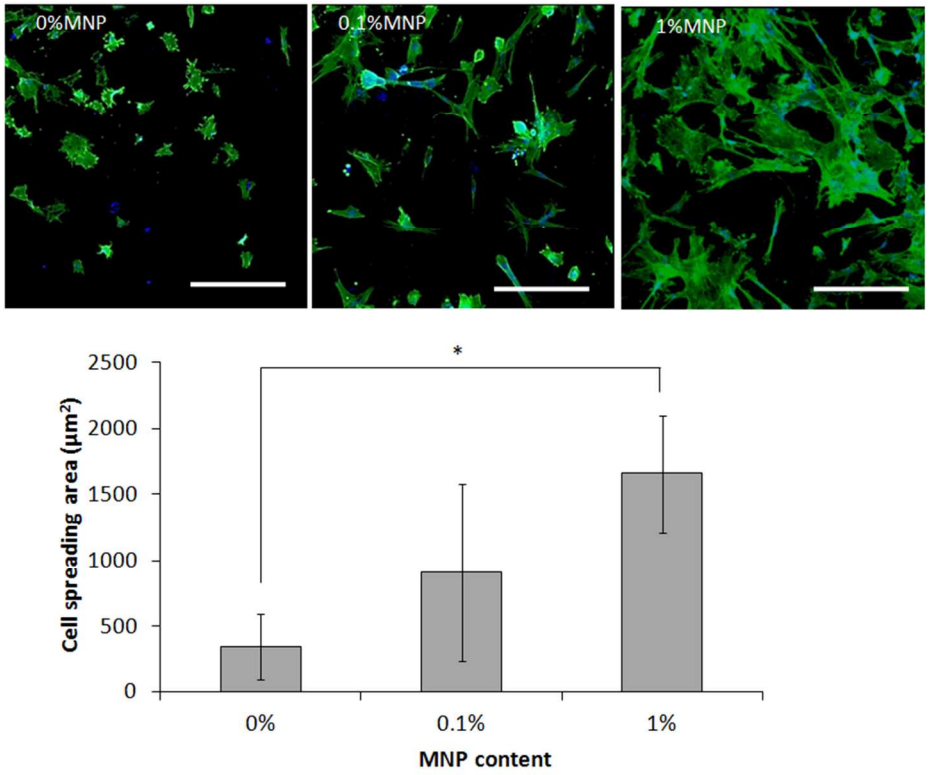

Figure 8. Cell adherence and spreading morphology at 6 h shown by fluorescence microscopy with the cell spreading area quantified. (Scale bar in the fluorescence images = 100 μm). Statistical significance difference was noted (*$p < 0.05$).

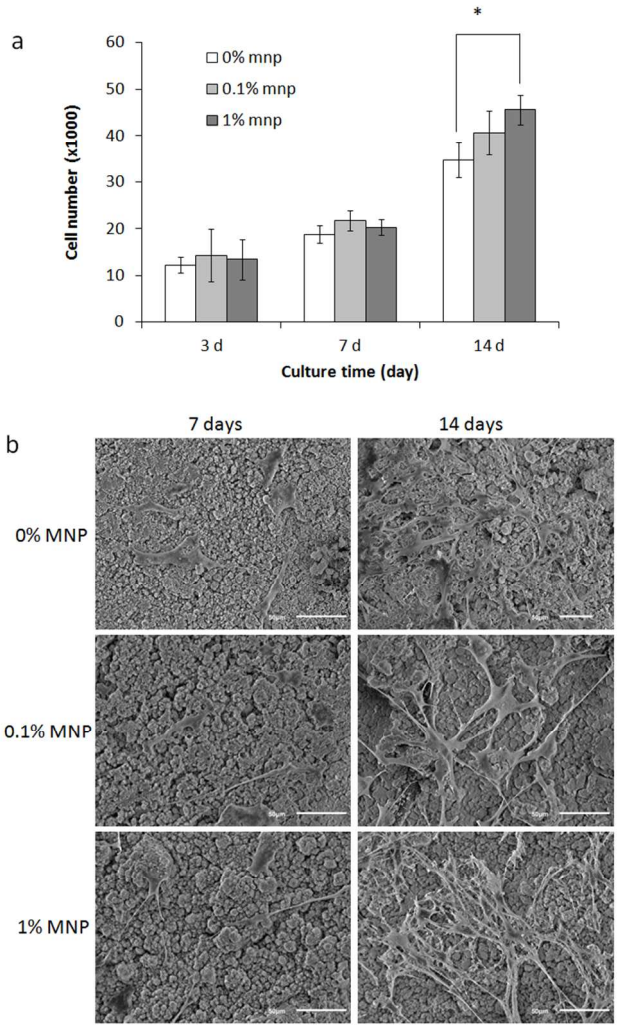

Figure 9. (a) Cell proliferation on the cement samples during culture for 3, 7, and 14 days, as measured by counting the cell number, and (b) cell growth morphology examined b SEM (scale bar = 50 μm). Statistical significance difference was noted (*$p < 0.05$).

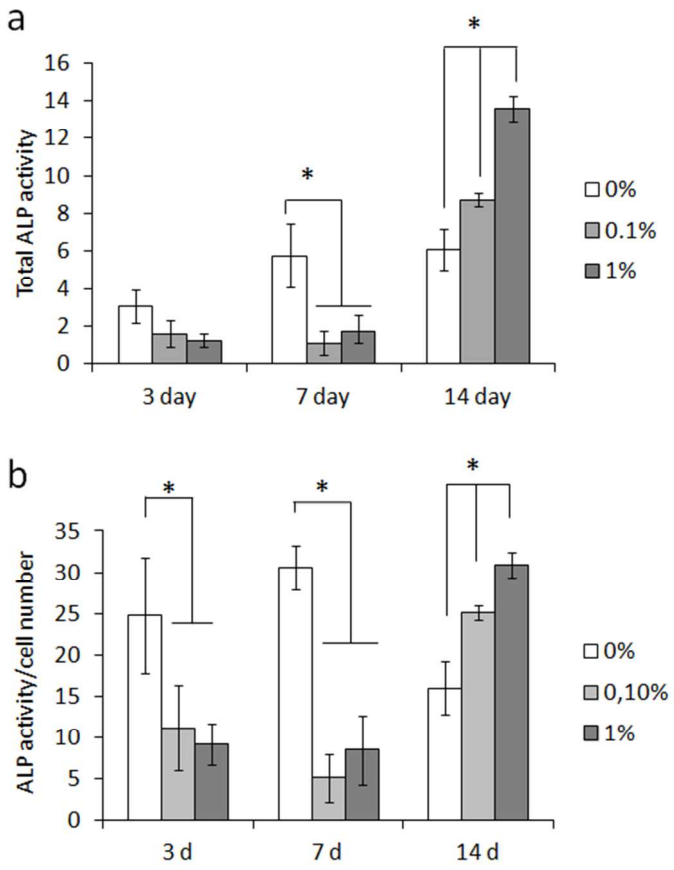

Figure 10. ALP activity of the cells; (a) total ALP and (b) normalized to cell number. Statistical significance difference was noted (*$p < 0.05$).